Title

Surface-bound FXIII enhances deposition and straightness of fibrin fibers

Journal

Biophysical Reports, 5(2)

ISSN

2667-0747

Authors

Awan, Myra

Papez, Maya

Walvekar, Ankita P

et al.

Publication Date

2025-06-01

DOI

10.1016/j.bpr.2025.100207

Biophysical Reports

ARTICLE

Surface-bound FXIII enhances deposition and straightness of fibrin fibers

Myra Awan,[1] Maya Papez,[1] Ankita P. Walvekar,[1] Sang-Joon J. Lee,[2] Kinjal Dasbiswas,[3] and Anand K. Ramasubramanian[1,*]

[1]Department of Chemical and Materials Engineering, San José State University, San José, California; [2]Department of Mechanical Engineering, San José State University, San José, California; and [3]Department of Physics, University of California, Merced, Merced, California

ABSTRACT Cross-linked fibrous networks are central to maintaining the structural integrity and functional relevance of many biological and engineered materials. Fibrin networks are the building blocks of blood clots, mediators of tissue injury and repair, and synthetic wound sealants. Cross-linking of fibrin fibers is catalyzed by the activated form of transglutaminase enzyme FXIIIa, which becomes available in plasma but is also readily presented on the surface of activated platelets and macrophages. The contribution of surface-bound FXIIIa to fibrin structure has not been well understood. In this work, we investigated the role of surface-bound FXIIIa on the formation and structure of fibrin fibers from FXIII-deficient plasma by confining the cross-linking reactions to the surface of microspheres. Quantitative microscopy revealed that cross-linking on FXIIIa-coated surfaces facilitates fibrin deposition following a sigmoidal kinetics, and that these fibers were straighter, longer, and more numerous compared with uncross-linked fibers bound to surfaces coated with anti-fibrin antibody. Our results suggest that, by modifying local fibrin density and structure, surface-bound FXIIIa may play a significant role in the mechanobiology of hemostasis and inflammation.

WHY IT MATTERS FXIII is a transglutaminase enzyme that catalyzes the formation of isopeptide bonds, i.e., cross-links, within and between fibrin fibers. The cross-links increase the mechanical and chemical stability of the fibrin networks. FXIII is present in plasma and is also expressed on the surface of activated platelets. Here, we used a platelet-free system and FXIII-deficient plasma to isolate the effect of surface-bound FXIII on the formation and structure of fibrin networks. We show that, even though cross-linking is limited to the surface, it has a significant impact on the length, curvature, rate, and amount of fibrin fibers formed in the surrounding environment. These results suggest mechanisms by which surface-bound FXIII influences the mechanobiology of blood clotting and wound healing processes.

INTRODUCTION

Fibrin is the key structural and functional component of blood clots, repairing and healing tissues, and also synthetic biopolymer scaffolds for diverse applications (1,2). Fibrin is a highly extensible, viscoelastic, strain-stiffening material with tunable properties that are conferred by its unique, hierarchical structure (3). The enzymatic release of fibrinopeptides A and B from fibrinogen by thrombin leads to noncovalent assembly of half-staggered fibrinogen molecules and the formation of protofibrils of ~25 nm diameter. The protofibrils pack by lateral aggregation into fibrin fibers that are a few hundred nanometers in diameter, where branching thereof yields a three-dimensional fibrin network. The network is strengthened by covalent linkages within and between protofibrils called cross-links (4,5). Before cross-linking, fibrin polymerization is reversible (6,7). After cross-linking, the polymerization becomes irreversible, and the network a mechanically and chemically more stable material (8–10). High compliance at small deformations is ideal for the compaction of fibrin clots by contractile forces generated by platelets or fibroblasts, while high stiffness at large deformations mitigates damage or rupture due to shear forces of blood flow or external tensile stress (11).

Cross-links are covalent ε-(γ-glutamyl)lysyl isopeptide bonds within and between the protofibrils. The

Submitted September 30, 2024, and accepted for publication March 20, 2025.

*Correspondence: anand.ramasubramanian@sjsu.edu

Myra Awan and Maya Papez authors contributed equally to this work.

Editor: Kandice Tanner.

https://doi.org/10.1016/j.bpr.2025.100207

cross-links are predominantly longitudinal γ-γ linkages within a strand, and transverse α-α linkages between strands. This coupling of constituent protofibrils compacts the fibrin fibers, densifies the network, and increases its mechanical and fibrinolytic resistance (12,13). Activated $FXIIIA_2$ (notated as FXIIIa (14)) is a transglutaminase enzyme responsible for the cross-linking of fibrin fibers (15). FXIII is present in plasma, and also in platelets and other cells of bone marrow origin. In plasma, FXIII is present bound to fibrinogen as inactive zymogen $FXIIIA_2B_2$, which is cleaved by thrombin in the presence of calcium to yield activated FXIIIa (16).

In contrast, the cellular form of FXIII is present in the cytoplasm as inactive FXIIIA, which is free from the B_2 subunit and is nonproteolytically activated by modest increase in intracellular Ca^{2+}. In response to activating stimulants, cellular FXIIIa is translocated to and retained on the outer cell surface, where it participates in cross-linking of several substrates including fibrin (5). Of interest, platelet cytoplasm carries large quantities of cellular FXIIIa, comprising 3% of their total protein content, at a concentration up to 150-fold higher than in plasma (17,18). It has been shown that thrombin/collagen stimulation translocates FXIIIa to the surface of procoagulant platelets, where it is retained and remains functional (19). The procoagulant platelets carry a FXIIIa-rich "cap" on their surface, which acts as a scaffold for platelet-driven fibrin fiber formation (20). Cellular FXIIIa from platelets has been shown to promote the formation of high-molecular-weight γ-dimers and α-multimers, cross-linking α_2-antiplasmin to fibrin, and stabilizing thrombi (21,22).

The fibrin fibers bound to the platelet surface are critical to the structural integrity and mechanical properties of the blood clots (23,24). As the clot forms, platelets reel the nascent fibrin fibers inward, thus remodeling local network architecture, increasing local fibrin density, and inducing prestress on platelet-bound fibers (25,26). We have recently shown that inhibition of plasma FXIIIa alters the nonlinear elastic properties of clots, causing them to soften at intermediate shear strain before showing the expected stiffening, where the softening is due to the easy bending and buckling of individual FXIIIa-inhibited fibrin fibers (27). The inhibition of FXIIIa also decreased platelet-fibrin interactions leading to a suggestion that fibrin cross-linking is essential to the transmission of platelet-induced prestress to the larger clot network (27,28). While these and other studies have unequivocally established the importance of fibrin cross-linking on clot properties, the relative contribution of cellular FXIIIa from platelets versus plasma FXIIIa to the structure and function of blood clots has not been well understood. FXIIIa distribution in clots is expected to be heterogeneous with higher concentrations in the platelet-rich regions of the clot. However, the impact of this nonuniformity due to platelet FXIIIa on fibrin network structure and mechanics is yet to be ascertained.

Investigating the impact of cross-linking due to platelet surface-bound FXIIIa on fibrin networks is complex because 1) spatiotemporal changes occur in the expression of FXIIIa on activated platelet surfaces (19,21), 2) FXIII-deficient human platelets are not readily available since FXIII deficiency is a rare disorder (29), and 3) in FXIIIa-deficient platelets derived from transgenic mice, other compensatory transglutaminases participate in cross-linking fibrin (30). As a first step toward characterizing the role of surface-bound FXIIIa on fibrin networks, here we isolate and examine its effect on fibrin formation and structure. To circumvent the aforementioned issues, we used FXIII-deficient plasma and a cell-free model system consisting of FXIIIa-bound microspheres instead of platelets. This allows us to isolate the effect of FXIIIa from confounding variables including expression of other surface-bound proteins such as fibrinogen, the variations in expression levels of FXIIIa depending on platelet activation status, mechanical deformations induced by platelet contractility, and membrane effects such as the redistribution of FXIIIa on lipid rafts. We analyzed fibrin cross-linking using fluorescence and electron microscopy to quantify the kinetics of formation and morphology of the fibrin fibers, thus providing insights into the role of surface-bound FXIIIa in clot and tissue mechanics.

MATERIALS AND METHODS

Materials

The materials were purchased from the following vendors: 6 μm carboxylated polystyrene microspheres (2.5%) and storage buffer from Polysciences (Warrington, PA); rabbit antihuman fibrin-E antibody, rabbit antihuman FXIIIa antibody, isotype IgG antibody, human FXIIIa, and human α-thrombin from Enzyme Research Laboratories (South Bend, IN); human factor XIII-deficient plasma from Assaypro (St Charles, MO); Alexa Fluor (AF) 594-conjugated fibrinogen from Invitrogen (ThermoFisher, Waltham, MA); tissue factor as prothrombin (PT) reagent from Dade Innovin (Siemens Healthcare Diagnostics, Tarrytown, NY); bovine serum albumin (BSA) solution, and calcium chloride from Sigma (St. Louis, MO); recombinant IL-10 from PeproTech (ThermoFisher, Waltham, MA); prostaglandin I_2 (PGI_2) from Cayman Chemicals; human monocytic cell line THP-1 (TIB-202) from ATCC (Manassas, VA); ibidi μ-Slide VI 0.4 and ibiTreat polymer coverslip from ibidi (ibidi USA, Fitchburg, WI); 2% glutaraldehyde solution in 0.1 M sodium cacodylate buffer, and 1% osmium tetroxide solution in 0.1 M sodium cacodylate buffer from Electron Microscopy Sciences (Hatfield, PA); MES buffer from Thermo Scientific (Waltham, MA). Carbodiimide solution (2%) was prepared by dissolving the required amount of 1-(3-dimethylaminopropyl)-3-ethyl carbodiimide hydrochloride in MES buffer; borate buffer at pH 8.5 was prepared by adding the required amount of 1 M NaOH to boric

acid. Pierce micro-BCA assay kit was from ThermoFisher (Waltham, MA).

Methods

Conjugation of antibodies and binding of FXIIIa to microspheres

Five hundred microliters of 2.5% carboxylated microspheres in 0.1 M carbonate buffer were washed with 0.1 M MES buffer three times by centrifugation for 5 min at 3000 rpm or 950 RCF (IEC Micromax RF Refrigerated Microcentrifuge, Thermo Fisher Scientific [Waltham, MA]). The resultant pellet was then reconstituted in 0.625 mL of 0.1 M MES buffer, to which 0.625 mL of 2% carbodiimide was added dropwise. Following a 20-min mixing period on a rocker, the mixture was washed three times by centrifugation for 5 min at 3000 rpm. Finally, the pellet was resuspended in 1.2 mL of 0.2 M borate buffer. To conjugate antibodies to these washed microspheres, 40 μg of isotype or anti-fibrin-E or anti-FXIIIa antibody was added, and incubated overnight at room temperature on a rocker. The conjugated microspheres were separated by centrifugation for 10 min at 3000 rpm, and the supernatant was saved for subsequent protein determination. To block the unreacted sites on the microsphere surface, the conjugated microspheres were reconstituted in 1.2 mL of 0.2 M borate buffer, supplemented with 50 μL of ethanolamine, and gently agitated for 20 min. The microspheres were centrifuged for 10 min at 3000 rpm and resuspended in 1 mL of 10 mg/mL BSA solution in 0.2 M borate buffer, followed by a meticulous 30-min mixing protocol at room temperature to preclude any nonspecific binding. The microspheres were centrifuged again for 5 min at 3000 rpm, reconstituted in 0.5 mL of storage buffer, and stored at 4°C until further use. To bind FXIIIa protein to the microspheres, 50 μL aliquots of both anti-FXIIIa antibody-conjugated and isotype antibody-conjugated carboxylated microspheres were incubated for 2 h with 80 μg/mL of FXIIIa (from a stock solution of 1.25 mg/mL) on a rocker in a light-protected environment at room temperature. After incubation, the microspheres were separated by a 5 min centrifugation at 3000 rpm, and the supernatant was reserved for protein determination. The microspheres were washed three times using 10 mg/mL BSA and 0.2 M borate buffer, and subsequently stored in the storage buffer at 4°C until further use. Protein content in the supernatant collected after antibody conjugation or FXIIIa binding was determined using Pierce micro-BCA assay following the manufacturer's protocols, and the extent of conjugation was calculated.

Clot formation with microspheres

Human factor XIII-deficient plasma (30 μL) was gently mixed with 1% v/v AF594-conjugated fibrinogen 1.5 mg/mL for 10 min at room temperature on a rocker in a light-protected environment. To this plasma, 3 μL of isotype antibody-conjugated-, anti-fibrin-E antibody-conjugated-, or FXIIIa-coated microsphere suspension was added. Clotting was initiated either by adding 20 mM $CaCl_2$ and 0.5 U/mL of thrombin or 1:12,800 dilution of PT reagent containing 200 ng/mL tissue factor, and 30 μL of the mixture was injected into ibidi μ-Slide VI 0.4 channels using an ibiTreat polymer coverslip.

Preparation of platelets and monocytes

Blood was obtained by phlebotomy after informed consent from healthy volunteers between age 20 and 30 years who did not have any known chronic cardiovascular conditions or medications known to alter platelet function (approved by San José State University IRB protocol F16134). The platelet pellet was obtained from platelet-poor plasma after the double centrifugation protocol as described previously (27). After removing the platelet-poor plasma supernatant, the platelet pellet was washed twice with Tyrode's buffer without calcium, supplemented with 1.25 μg/mL prostaglandin (PGI_2). The platelets were used within 3 h of blood draw. THP-1 cells were subcultured following the vendor's recommendation and protocols as described previously (31). The cells were activated with 100 ng/mL of IL-10 for 24 h to upregulate the expression of FXIIIa (32). Anti-FXIIIa-antibody or isotype antibody (120 μg/mL) was added to the platelet or to the monocyte suspension in FXIII-deficient plasma and incubated for 10 min at room temperature. Clotting was initiated with 0.5 U/mL thrombin and 20 mM calcium chloride. After 1 h, the clots were fixed as described below.

Visualization of clot microstructure and ultrastructure

To visualize clot structure, the channels containing clots were placed on a microscope stage and imaged either at 63× magnification (DMi8, Leica Microsystems, Deerfield, IL) or at 100× (LSM 700, Zeiss, Dublin, CA), using oil immersion objectives. After allowing 2 min for thrombin-induced gelation or 5 min for tissue factor-induced gelation, images were captured at the same location at 1-min intervals for 15 min. This gelation period was essential for the microspheres to remain stationary due to entrapment. The three-dimensional image stacks acquired by confocal imaging were visualized and processed in an Imaris v9.6 (Oxford Instruments, Pleasanton, CA) for normalization using the integrated background subtraction feature. To visualize clot ultrastructure, clot formation was initiated as described previously, and 15 μL of the mixture was spread on an ibiTreat polymer coverslip. After 20 min of gelation, the clots were fixed for 2 h using 2% glutaraldehyde in 0.1 M sodium cacodylate buffer at a pH of 7.2, washed three times for 10 min each in 0.1 M sodium cacodylate buffer at the same pH. The clots were incubated for 2 h in 1% osmium tetroxide in 0.1 M sodium cacodylate buffer at pH 7.2, followed by another round of three washes for 5 min each. The clots were dehydrated by sequential immersion in 35, 50, 70, 80, 95%, and two rounds of 100% ethanol for 10 min each. The dehydrated specimens were then critical point-dried for 60 min, and mounted onto stubs using conductive carbon dots. The specimens were sputter coated with gold for a thickness of 2 nm. The specimens were then loaded onto a stub shuttle and visualized on a scanning electron microscope at 1 keV (GeminiSEM 460, Zeiss, Dublin, CA).

Image analysis

Images of clot microstructure and ultrastructure were analyzed using the various plug-ins available on Fiji ImageJ. The RGB images were converted to monochromatic images by splitting into separate channels. The blue and red channels displayed varying fluorescent intensity values, corresponding to microsphere and fibrin fluorescence, respectively. To remove the microsphere from image analysis, the intensity of the blue channel was subtracted from the red channel, effectively eliminating the microsphere while preserving the fibrin intensities. Intensity profiles of fibrin were obtained at four orthogonal directions around the microsphere, spanning from the center to the surface, to a distance of 21 μm when fluorescence intensities have faded down to background values, and averaged. The exponential decay function with distance, the integral of fluorescence intensity, and Hill function were estimated using MATLAB 2024b.

For SEM ultrastructure examination, we employed kappa analysis using the ImageJ plugin. This approach allowed us to assess curvature, fiber length, and fiber count. Fiber length was calculated as the length of the section of the fiber between the last attachment point on the microsphere surface to the first branchpoint outside the microsphere. The curvature was estimated for the same section. B-Spline curvature paths were created to trace each fiber on the microsphere surface, facilitating a complete analysis of its

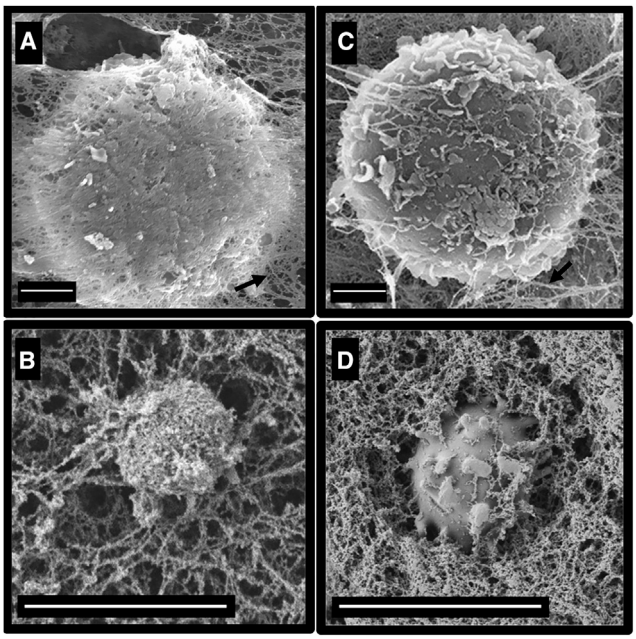

FIGURE 1 Fibrin fiber network connected to activated macrophage (*A*) and platelet (*B*) surfaces, while treatment with FXIIIa antibody (*C* and *D*) abrogates fibrin interactions with the cell surfaces. Scale bars, 2 μm.

structural trajectory. The plug-in provided the local ("point") curvature value along the trajectory of the curve. The entire trace was divided into 250 equal segments, and the curvature at each of those points was estimated by the plug-in (33).

Statistical analysis

All microsphere experiments were performed in four to seven independent replicates with the microspheres conjugated in three separate batches. The platelet and monocyte experiments were performed in triplicates. Statistical significance was tested using Student's *t*-test in Microsoft Excel.

RESULTS

Effect of cellular FXIIIa on fibrin networks

FXIIIa is expressed by cells of bone marrow origin, including monocytes and platelets (34,35). Functional FXIIIa levels are shown to be upregulated on the surface of monocytes activated with IL-4 and IL-10 (32). Abundant FXIIIa has been detected on the surface of platelets activated with thrombin and collagen (19). Both macrophages and activated platelets express receptors (CD11b/18 and CD41/61) that bind to fibrin (ogen) (36). We examined if FXIIIa expressed on the surface of platelets and macrophages can cross-link fibrin bound to these cells. We used FXIII-deficient plasma to isolate the effect of surface-bound FXIIIa. We used SEM to visualize the nature of the fibrin network that is attached to FXIIIa expressed on the surface of activated platelets and monocytes. As shown in Fig. 1, we observed that the fibrin networks attached to the surface of activated macrophages and platelets appear to emanate radially in bundles (particularly on the monocyte surface, as shown by *arrows*). Such fibers were absent when the monocytes and platelets were treated with a blocking antibody against FXIIIa. These results indicate that the cross-linking of fibrin by FXIIIa expressed on the cell surface modifies the structure of fibrin networks immediately adjacent to the cells.

Kinetics of fibrin deposition on FXIIIa-coated and anti-fibrin E-antibody-coated microspheres

To examine the effect of surface-bound FXIIIa on the cross-linking of fibrin fibers, we used a cell-free system that will isolate the effects of cross-linking and provide ample control and consistency on FXIIIa expression on the cell surface. We used FXIIIa-coated microspheres that will mediate fibrin cross-linking on the surface, and microspheres coated with anti-fibrin E antibody (anti-fnE-Ab), which binds to the fibrin E domain but does not cross-link the fibers. As a negative control, we used microspheres coated with isotype antibody to quantify passive interaction. Using protein measurements in solution and mass balance, we determined that the microsphere surfaces were nearly fully conjugated with the antibodies (Fig. S1). We also used FXIII-deficient plasma to ensure that, upon activation with thrombin, the cross-linking reactions are restricted to the microsphere surface, and do not occur in the bulk. We used confocal fluorescence microscopy to visualize fibrin fibers near the microspheres (Fig. 2). As expected, the fibrin fibers did not interact with beads coated with isotype antibody indicating minimal nonspecific interactions. In contrast, the fibrin fibers were bound to the anti-fnE-Ab-coated microspheres, as seen by the interaction between the fibers and the microspheres; and these interactions are uneven in patches as seen by the colocalization of the blue and red fluorescence. The fibrin fibers appeared to interact more strongly with FXIIIa-coated microspheres, and the thickness of the fibrin fibers appeared to be higher and more uniformly distributed. These qualitative observations suggest that, similar to those seen on cell surfaces, the fibers interacting with FXIIIa-coated surfaces also appeared to emanate as a bundle of fibers.

To understand the biophysical mechanisms of fibrin cross-linking on FXIIIa-coated surfaces, we monitored the kinetics of fibrin deposition on FXIIIa- and anti-fnE-Ab-coated microspheres (Fig. S2). To quantify the fibrin deposition, we focused on single microspheres within the field of view. Over the course of 20 min after

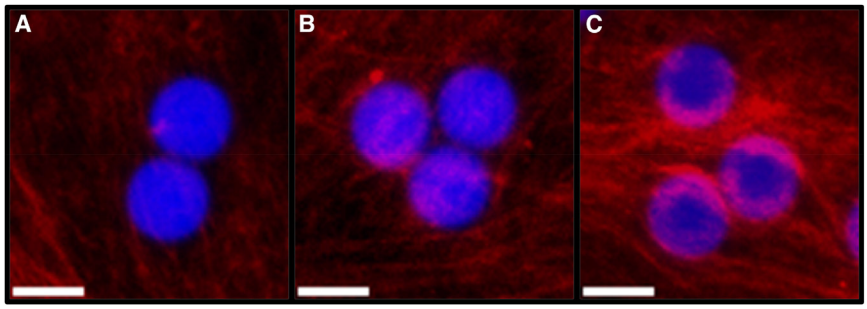

FIGURE 2 Fibrin fibers (*red*) do not interact with microspheres (*blue*) coated with isotype antibody (*A*) but interacts with microspheres coated with anti-fibrin E antibody (*B*) or with FXIIIa (*C*). Fibrin fibers are thickly distributed and wrapped around FXIIIa-coated microspheres. Scale bars, 5 μm.

the initiation of clotting with thrombin and calcium, fibrin deposition on the microspheres was monitored from the increase in fluorescence intensity around the microspheres (Fig. 3, *A* and *B*). On comparing fluorescence intensities between the two images, it is evident that fibrin deposition on the anti-fnE-coated surface is higher at earlier times than the FXIIIa-coated surface. This may be attributed to the immediate binding of fibrin to the antibody on the microsphere surface. However, at the end of the clotting duration, the fluorescence intensity on the FXIIIa-coated surface is higher than on the anti-fnE-coated surface. We averaged the fluorescence intensities in four different directions around the microspheres at different time points (Fig. S3). The fluorescence intensity around the isotype-Ab-coated surface was barely higher than the background intensity far from the microsphere, indicating the minimal nonspecific interaction between fibrin fibers and the microspheres (Fig. S3). The background fluorescence intensities in the bulk were subtracted from the fluorescence intensities around FXIIIa- and anti-fnE-Ab-coated surfaces to obtain the change in fluorescence intensity only due to fibrin deposition on the surface. The spatiotemporal changes in fibrin deposition (Fig. 3, *C* and *D*) shows that fibrin density decreases with distance from the microsphere surface, and density at any given distance increases as clotting proceeds. The increase in fluorescence intensity on the surface is significantly higher on the FXIIIa-coated surface than on the anti-fnE-Ab-coated surface. The increase in fluorescence due to fibrin binding to or cross-linking on the surface can be seen over a distance of $\sim$5 μm into the bulk.

To quantitatively define the spatiotemporal dynamics of fibrin deposition, we fitted the fluorescence intensity as an exponential decay function of distance from the surface, $I(r,t) = I_S(t)\, e^{-r/\delta(t)}$, where $I_S(t)$ and $\delta(t)$ represent the fluorescence intensity on the bead surface, and the characteristic decay length, respectively. $I_S(t)$ serves as a surrogate measure of fibrin level on the surface due to binding or cross-linking, while $\delta(t)$ is the length over which the surface effects of fibrin binding or cross-linking are felt into the bulk.

As shown in Fig. 3 *E*, as clotting proceeds, the intensity on the anti-fnE-Ab-coated surface changes immediately followed by a modest increase. By contrast the fluorescence intensity on the FXIIIa-coated surface is low initially but, upon reaching a threshold level, increases rapidly before saturating, demonstrating overall sigmoidal kinetics. The immediate increase in fluorescence intensity on the anti-fnE-Ab-coated surface is due to the attachment of fibrin polymers as soon as they are formed, while the sigmoid kinetics on the FXIIIa-coated surface implies autocatalytic fibrin deposition. We also estimated the total amount of fibrin deposited (Γ) around the microsphere by integrating the area under the fluorescence intensity curve over an operational threshold of 2 μm from the surface. Fig. 3 *F* shows that, although the total amount of fibrin deposited on FXIIIa-coated surface is low initially, at the end of the clotting period similar amounts of fibrin deposited on the two surfaces. This indicates that FXIIIa-catalyzed cross-linking on the surface is just as effective as the antibody-mediated covalent attachment of fibrin in terms of total amount of fibrin formed near the surface. Fig. 3 *G* shows that, while the decay length for anti-fnE-Ab changes only modestly, that on the FXIIIa-coated surface decreases with time, indicating the spatially increasing steepness of the intensity profile. In other words, as clotting proceeds, the fluorescence intensity of fibrin close to the cross-linked surface increases faster than the increase in the bulk. Compared with Fig. 3 *F*, since the total amount of fibrin polymerized is the same in both uncross-linked and cross-linked cases, Fig. 3 *G* shows that surface cross-linking increases fibrin deposition closer to the surface than elsewhere.

To obtain insights into the kinetics of fibrin deposition on FXIIIa-coated surfaces, we fitted the experimental data on fluorescence intensity on microsphere surface, $I_S(t)$, to a three-parameter logistic function given by: $I_S(t) = \dfrac{I_{max}}{1+\left(\dfrac{I_{max}}{I_{min}}-1\right)e^{-t/\tau}}$, where τ is shape factor (a characteristic timescale for exponential

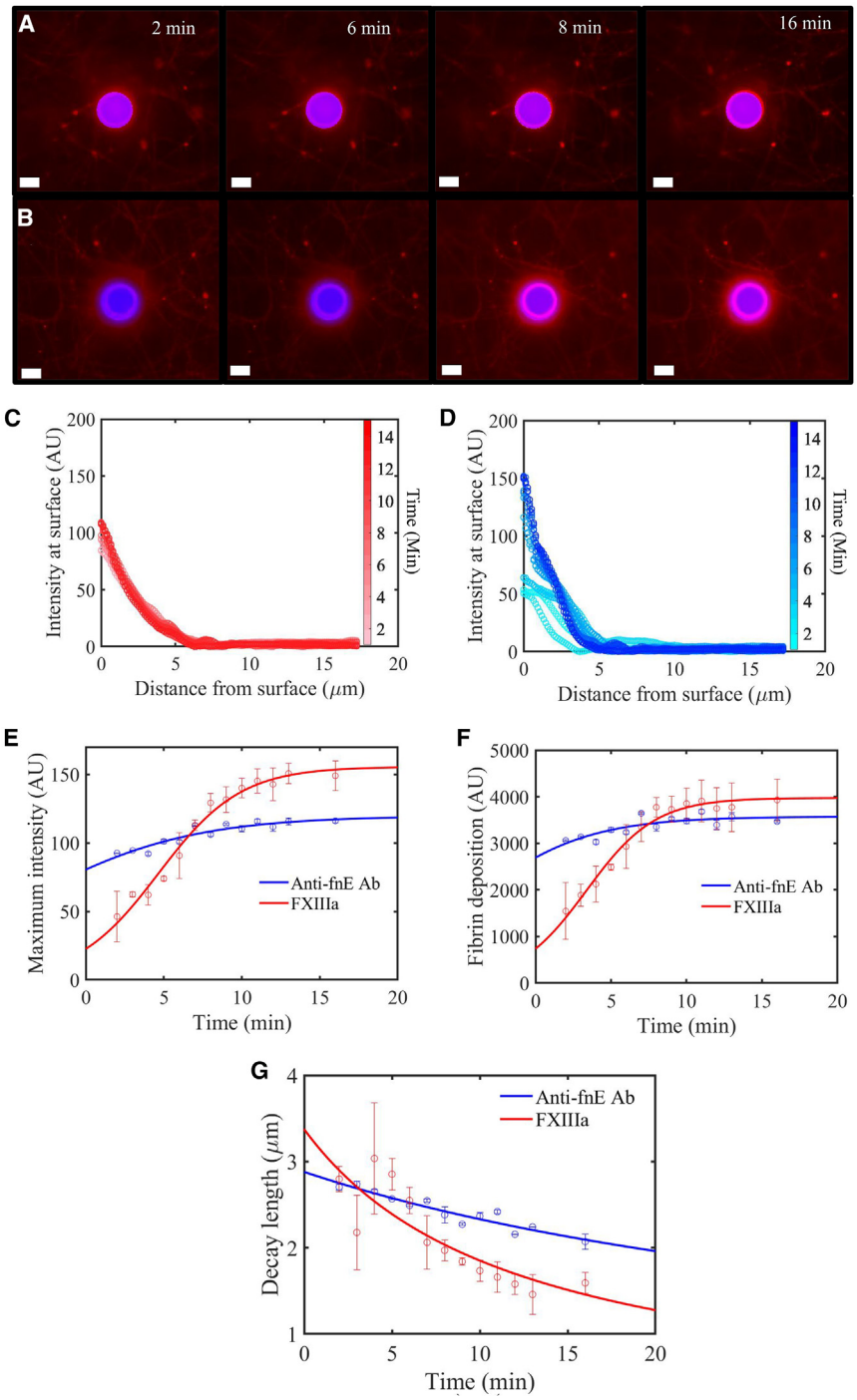

FIGURE 3 Kinetics of fibrin formation on microspheres from FXIII-deficient plasma when clotting was initiated with thrombin. (*A* and *B*) Time-lapse fluorescence microscopy reveals increase in fibrin deposition over 20 min, as visualized using AF594-conjugated fibrinogen (*red*) on microsphere surface (*blue*) coated with anti-fnE-Ab (*A*) for FXIIIa (*B*). The images are normalized to the background intensities. (*C* and *D*) Fibrin intensity variation with distance from the surface to background over time on surfaces coated with anti-fnE-Ab (*C*) for FXIIIa (*D*). Time dependence of (*E*) maximum fluorescence intensity on the microsphere surfaces ($N = 4$ microspheres, mean $\pm$ SD), (*F*) total amount of fibrin deposited over a 2 μm distance from the surface, and (*G*) decay length of fluorescence intensity.

growth), and I_{min} and I_{max} are the minimum and maximum fluorescence intensities at the initial ($t = 0$) and late times ($t \to \infty$), respectively. The excellent fit to the logistic function suggests that fluorescence intensity on the microsphere surface is governed by the logistic growth kinetics, $\frac{dI_S}{dt} = \frac{I_S(I_{max} - I_S)}{\tau\, I_{max}}$. This equation implies that fibrin deposition on the microsphere surface is driven by the binding of fibrin that is already deposited on the surface (I_S), to fibrin that is yet to be deposited from the bulk ($I_{max} - I_S$), with an apparent binding rate constant ($1/\tau$), which gives the shape factor of the logistic function. I_{max} is related to the amount of FXIIIa available for fibrin cross-linking on the surface. It should be noted that, although FXIIIa does not irreversibly bind to fibrin and its level should remain constant, the cross-linking of fibrin increases the density

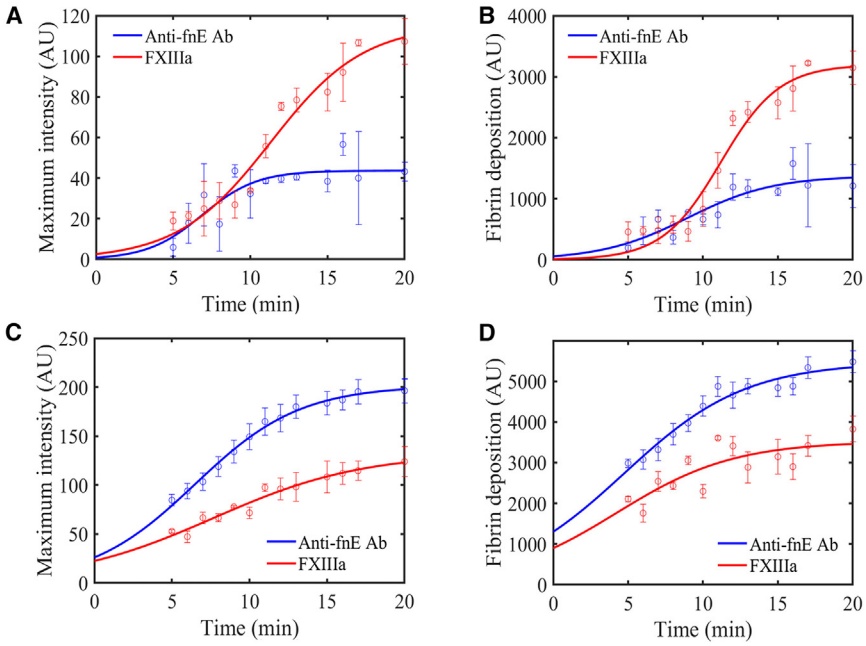

FIGURE 4 Kinetics of fibrin formation on microspheres from FXIII-deficient plasma (*A* and *B*) and FXIII-supplemented plasma (*C* and *D*) when clotting was initiated with tissue factor. (*A* and *C*) Maximum fluorescence intensity on the microsphere surfaces; (*C* and *D*) total amount of fibrin deposited over a 2 μm distance from the surface ($N = 4$, mean $\pm$ SD).

near the microsphere over time, leading to a gradual decrease in the availability of FXIIIa due to steric hindrance. The fibrin deposition curves, $\Gamma(t)$, on the microsphere surfaces also follow profiles similar to that of $I_S(t)$.

Kinetics of fibrin deposition in the absence and presence of plasma FXIIIa

We also monitored the kinetics of fibrin deposition on the microsphere surfaces using tissue factor as initiator, as a physiologically more relevant case of in situ thrombin generation. The kinetic profile of fluorescence increase due to fibrin formation shows exponential decay with distance from the microsphere surface, similar to that of initiation with exogenous thrombin (Fig. S4). The increase in fluorescence intensity on the microsphere surface coated with FXIIIa demonstrates a sigmoidal curve (Fig. 4, *A* and *B*), but that on the anti-fnE-Ab-coated surface shows saturation kinetics. Unlike initiation with thrombin, initiation with tissue factor resulted in a lower start to fibrin deposition and lower amount deposited on the anti-fnE-Ab-coated surface. This is due to the initially limited availability of thrombin, and therefore slower fibrin polymerization. In addition, although the deposition starts slow on the FXIIIa-coated surface, the final fluorescence intensity is 2.5-fold higher on the FXIIIa-coated surface than on the anti-fnE-Ab-coated surface. The effect of increase in fibrin on the FXIIIa-coated surface propagates farther from the surface, as seen by a 2.5-fold higher fibrin deposition over a distance of 2 μm from the FXIIIa-coated surface than from the anti-fnE-Ab-coated surface.

Sigmoidal curves with an initial lag phase, subsequent exponential growth, and a final equilibrium phase that is seen here in FXIIIa-coated microspheres has also been observed in other systems with a nucleation-dependent elongation model of fibril formation (37). The shape factor, τ, is essentially the time duration over which $I_S(t)$ or $\Gamma(t)$ increases exponentially, i.e., smaller τ implies that the transition from a low to a high value occurs in a shorter time. We defined lag time as $(t_{50} - \tau)$, where $t_{50} = \tau \exp(I_{max}/I_{min} - 1)$ is the time taken to reach 50% of $I_{max} - I_{min}$. The values of τ for fluorescence intensity and deposition on the FXIIIa-coated microsphere surface are nearly similar when clotting is initiated with thrombin (2.6 $\pm$ 0.3 min) or with tissue factor (3.0 $\pm$ 0.5 min). The respective lag times were estimated to be 2.0 and 8.3 min, which is consistent with faster fibrin polymerization with thrombin than with tissue factor. However, the similar τ values between the two cases suggests that cross-linking by FXIIIa, not fibrin polymerization, limits the rate of deposition since, as fibrin polymerization proceeds, more fibrin oligomers and nascent protofibrils get cross-linked by surface FXIIIa before they are fully polymerized. Thus, cross-linking effectively controls fibrin deposition on the surface independently of polymerization.

The experiments described so far were performed in FXIII-free plasma to isolate the effect of surface immobilized FXIIIa on fibrin cross-linking *at the*

surface. To examine the impact of FXIIIa in plasma on modulating the interaction of fibrin with FXIIIa on surface, we monitored the kinetics of fibrin deposition from FXIII-free plasma supplemented with a physiologically relevant concentration of 10 μg/mL FXIIIa using tissue factor as the initiator. As shown in Fig. S4, the fluorescence intensity decreases exponentially with distance from the microsphere surface, although the intensities (even after background subtraction) were higher than for the case in the absence of FXIIIa. As Fig. 4, *C* and *D* show, upon supplementation with FXIIIa, fluorescence intensity on anti-FnE-Ab-coated surfaces is drastically increased and is higher than on FXIIIa-coated surfaces. Under these conditions, the total amount of fibrin deposited on the microsphere surfaces was also higher on the anti-FnE-Ab-coated surface compared with the FXIIIa-coated surface. The deposition profiles follow saturation kinetics instead of sigmoidal kinetics. These results demonstrate that cross-linking in solution appreciably alters the effects of cross-linking on a surface presenting FXIII. Cross-linking in solution increases the avidity of fibrin E domains in a fiber, which can bind rapidly to anti-FnE-Ab-coated surfaces, thus resulting in the most deposition. Cross-linking in solution also reduces the number of cross-linking sites available for cross-linking on the FXIIIa-coated surface, thus resulting in the least deposition. It should also be noted that the abundance of plasma FXIIIa does not eliminate the increase in fluorescence intensity on FXIIIa-coated surfaces, indicating that fibrin cross-linking reactions still happen on FXIIIa-coated surfaces.

Characteristics of fibrin fibers on FXIIIa-coated and anti-fibrin-E-antibody-coated surfaces

Having established distinct differences between the kinetics and amount of fibrin deposition by binding and by cross-linking, we sought to distinguish the characteristics of individual fibrin fibers cross-linked by FXIIIa on the surface from those that were bound to the surface by fibrin-E antibody. We examined the morphology of single fibers connected to the microsphere surfaces using SEM (Fig. S5). Fig. 5 *A* shows that fibrin is seen bound to anti-fibrin E-coated surfaces as individual fibers. On the microsphere surface, fibers were sparse, and were connected to the rest of the network through a few short, single fibers. In contrast, Fig. 5 *B* shows that FXIIIa-coated microspheres were more deeply integrated with the surrounding network. Fibrin cross-linked to FXIIIa-coated surfaces presented as fibers that are long and continuous, and closely packed like sheets; and were connected to the rest of the network through several long networks of fibers, similar to what is seen in Fig. 1 on FXIIIa-presenting cell surfaces. Fig. S6 shows that isotype antibody-coated microspheres were uniformly covered with the fibrin network. The fibrin fibers appear to follow the contour of the microsphere (in contrast to Figs. 5 *B* and S5), which suggests that interactions are nonspecific due to volume exclusion. We quantified the morphology of the fibrin fibers attached to the microspheres. We observed that 50% more fibers attached when cross-linked on the surface compared with binding on the surface without cross-linking (25.50 ± 6.11 vs. 17.11 ± 5.5, Fig. 5 *C*). We also observed that the fibers cross-linked on the surface were longer than those bound to antibody-coated surfaces (Fig. 5 *D*). The fiber lengths were fit to a lognormal distribution, with the median length of fibers cross-linked on the surface being twofold higher than that of fibers bound to the surface (0.88 ± 0.01 vs. 1.77 ± 0.02 μm, $p < 0.05$). Several long fibers with lengths three times more than the average length of the fibers ($\sim$15 μm) were seen when cross-linked on the surface while no such long fibers were seen emanating from uncross-linked fibers bound to the microsphere surface.

To gain insights into the persistence length of the fibers, we traced the curvature of the fibers attached to the microsphere surfaces along their arc length. As shown for representative fibers in Fig. 5, *E* and *F*, the local curvature with larger and smaller values representing local bending and straightening of the fibers, respectively. The local curvatures of uncross-linked fibers were one or two orders of magnitude larger than for cross-linked fibers, indicating that the cross-linked fibers were a lot straighter. The distribution of maximum curvatures (95th percentile) of all fibers shows that the fibers cross-linked on the surface were much less flexible than fibers that were bound to antibody-coated surfaces (Fig. 5 *G*). The uncross-linked fibers show a bimodal distribution with the smaller mode overlapping with cross-linked fibers, and another significantly larger mode indicative of higher tortuosity. As shown in Fig. 5 *H*, the local curvature of the cross-linked fibers was a minimum on the microsphere surface, and it increases sevreralfold moving farther from the surface as the fibers indicating that the fibers become more flexible. As shown in the inset of Fig. 5 *H*, the local curvature of the uncross-linked fibers attached to anti-fnE-Ab-coated microspheres also increases farther from the surface, although the increase is an order of magnitude larger over a shorter distance than for the cross-linked fibers. These observations indicate that the cross-linking reaction on the surface is sufficient to generate fibers that are

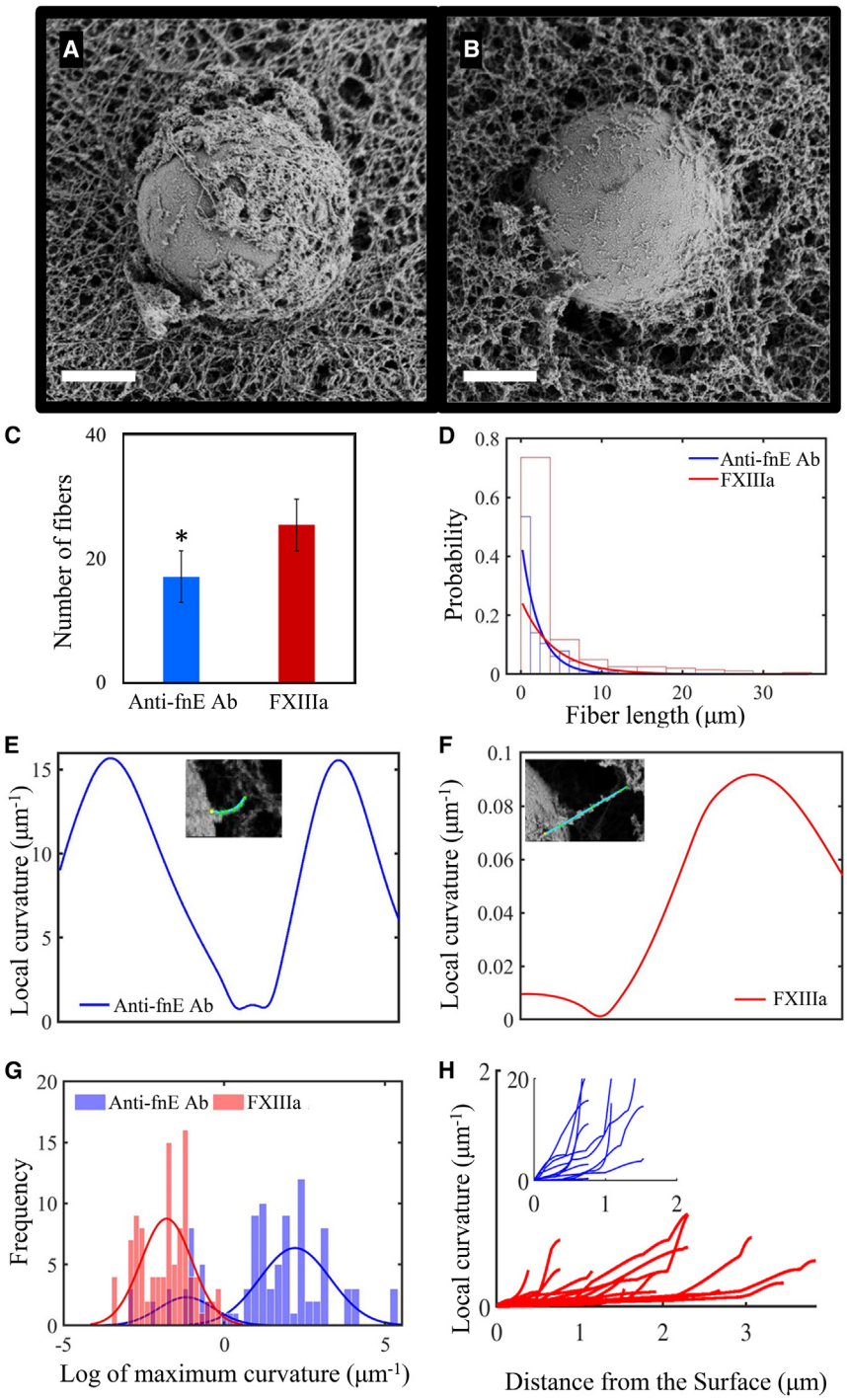

FIGURE 5 Ultrastructure of fibrin fibers bound to anti-FnE-Ab-coated microspheres (*A*) or cross-linked on FXIIIa-coated microspheres (*B*). Scale bars, 2 μm. Number (*C*) and length (*D*) of fibers connected to the microspheres ($n = 96$ and 178 fibers, $N = 6$ microspheres, mean $\pm$ SD, $p < 0.05$ for *C*). (*E* and *F*) Local curvature of representative fibers (*inset*) attached to the microspheres along the fiber length. (*G*) Distribution of maximum local curvature of the individual fibers attached to the microspheres. (*H*) Local curvatures of fibers cross-linked on FXIIIa-coated microspheres or uncross-linked fibers (*inset*) ($n = 17$).

significantly straighter and longer, which extend for a few microns into the bulk.

Fibers cross-linked, but not bound, to the surface span neighboring microspheres

Since the length of fibrin fibers cross-linked on the microspheres are straighter and a few microns long, we considered if the cross-linking of the fibers on the surface may promote interactions between two such surfaces. In SEM micrographs, we observed several clusters of FXIIIa-coated microspheres that were enmeshed in the matrix (Fig. 6 *A*). The microspheres, although not in contact with each other, were seen to be connected by several long individual fibrin fibers (27 $\pm$ 9 fibers, 1.62 $\pm$ 0.76 μm, $N = 3$ microspheres).

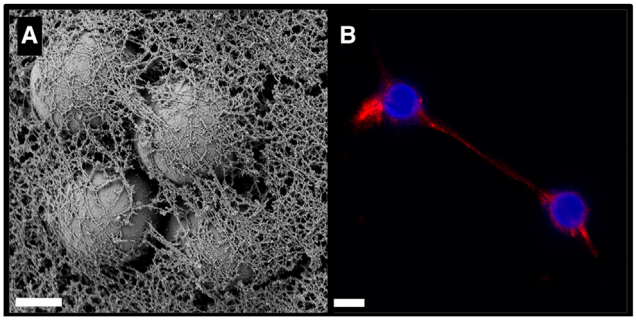

FIGURE 6 Fibrin fibers cross-linked connect FXIIIa-coated microspheres. Scale bars, 2 μm (*A*) and 5 μm (*B*).

The cluster of FXIIIa-coated microspheres appeared to be truly integrated into the network rather than passively encapsulated. In contrast, only negligibly small and short fibrin fibers were seen between clusters of anti-fnE-Ab-coated microspheres (Fig. S7). To visualize interactions that are located farther than observable in an SEM, we visualized pairs of FXIIIa-coated microspheres using confocal microscopy (Fig. 6 *B*). Some of the microspheres that were located at distances of several tens of microns from each other were connected by fibrin fibers (41.8 $\pm$ 25.7 μm, $N = 3$). In addition, these fibers also appear straight and stretched between the two connecting microspheres. This observation suggests the possibility that the presence of FXIIIa on two surfaces separated by a certain distance may serve to nucleate two partially cross-linked protofibrils that laterally aggregate to grow into continuous fibers.

DISCUSSION

In this work, we have shown that cross-linking of fibrin fibers only on a surface results in higher fibrin deposition compared with the binding of uncross-linked fibers to the surface. Furthermore, cross-linking on the surface results in a denser fibrin network composed of straight fibers that may span a few microns. In other words, FXIII bound to the surface impacts fibrin structure and density far from the surface.

By using a platelet-free system and FXIII-deficient plasma, we eliminated any influence of time- and agonist dose-dependent upregulation of fibrinogen and FXIIIa on the surface of activated platelets, and that of plasma FXIIIa on fibrin cross-linking, respectively. Since FXIIIa is bound to fibrinogen through the FXIII-B as $FXIIIA_2B_2$ complex, and in our experiments only FXIIIa is immobilized on the microspheres, fibrin binds to the microsphere surface. Therefore, fibrin deposited on the surface is not due to direct attachment but due to the compaction of the protofibrils that results from cross-linking. As seen in the clot microstructure images in Figs. 2 and 6, the impact of surface cross-linking extends several microns away from the surface when compared with isotype antibody-coated surfaces wherein fibrin fibers do not attach to the surface and the intensity is the same near the surface as it is in the bulk (Fig. S2). Furthermore, the compaction of fibrin fibers due to cross-linking on FXIIIa-coated surfaces results in more fiber deposition than due to the binding of uncross-linked fibrin fibers to the antibody-coated surfaces (38). The sharp sigmoidal profile in fibrin deposition with time on FXIIIa-coated surfaces demonstrates an autocatalytic-like process: after a slow initial phase of fibrin deposition by cross-linking, the rate of deposition quickly accelerates due to the enhancement in the rates of lateral aggregation to existing cross-linked protofibril segments. In contrast, the deposition of fibrin fibers on antibody-coated microspheres showed immediate binding followed by saturation kinetics. In this case, the fast binding of fibrin monomers and oligomers to the antibody-coated surface rapidly increases the local concentration of these species but the lack of cross-linking is insufficient for enhancing the lateral aggregation and compaction of protofibrils.

Although fibrin polymerization and cross-linking reactions follow complex multiphasic kinetics, the published data on rates of reactions under controlled settings can provide a conceptual model of how cross-linking of fibrin fibers on the surface may influence the growth of the fibers around the surface (Fig. 7). Both fibrin polymerization and cross-linking are sequential processes, with similar rates. The protease thrombin cleaves ($k_{cat}/K_M \sim 10\ \mu M^{-1}\ s^{-1}$) fibrinopeptide B from fibrinogen (f_{AB}) to yield fibrin-A monomer (f_A), which reversibly self-associates to form fibrin-A oligomer (39). Thrombin also cleaves fibrinopeptide A from fibrin-A oligomers at a similar rate ($k_{cat}/K_M \sim 4\ \mu M^{-1}\ s^{-1}$) to yield fibrin ($f$) oligomers. Although not experimentally determined, the nonenzymatic association of f oligomers to form protofibrils, and the extension of protofibrils to form fibers is estimated to be similar to that of enzymatic reactions ($\sim$1–30 $\mu M^{-1}\ s^{-1}$) (40). In parallel, the transglutaminase FXIIIa longitudinally cross-links the γ chains in f_A and f oligomers relatively rapidly ($k_{cat}/K_M \sim 5\ \mu M^{-1}\ s^{-1}$) (41), and transversely cross-links α chains between adjacent protofibrils at a much slower rate ($k_{cat}/K_M \sim 0.007\ \mu M^{-1}\ s^{-1}$). In our system, since fibrinogen concentration is $\sim$10 μM, the timescale of fibrin monomer generation is of the order of seconds, and the generation of protofibrils will be of the order of minutes, which is consistent with experimental observation. As thrombin generates f_A and f oligomers, the first layer of oligomers and protofibrils are assembled near the microsphere surface. Since the

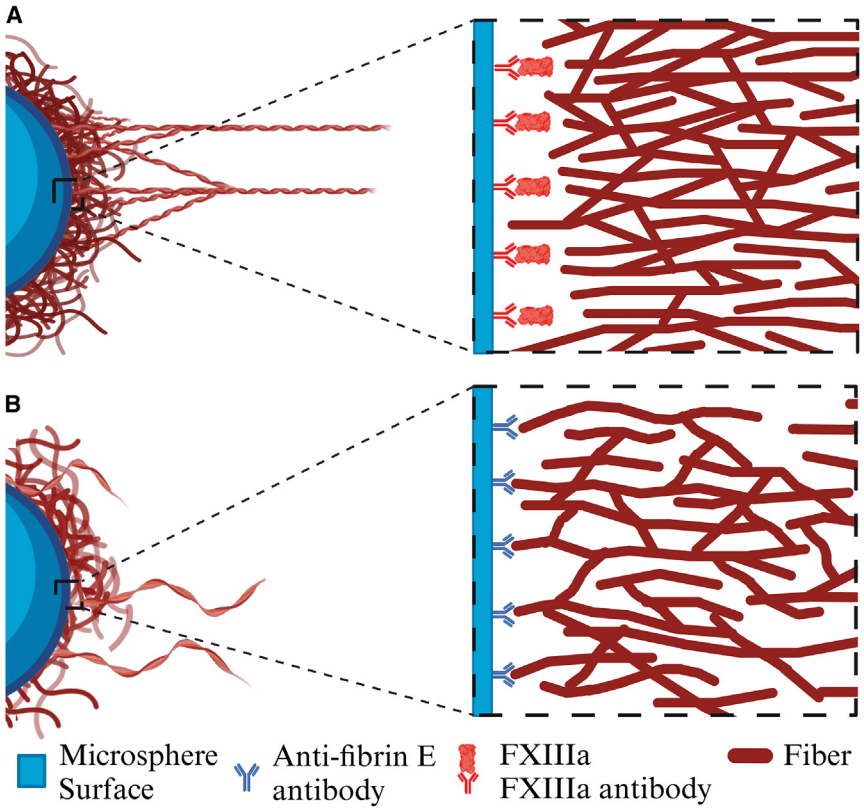

FIGURE 7 A model for fibrin cross-linking on FXIIIa-bound surfaces. As fibrin oligomers and protofibrils are polymerized in solution, those close to the surface get cross-linked on the surface on FXIIIa-coated surfaces (*A*). The cross-linking straightens the protofibrils and promotes the aggregation of protofibrils as they are formed in solution, leading to increased fiber density on the surface, and those close to anti-fnE-antibody-coated surface bind to the surface (*B*). The uncross-linked protofibrils remain tortuous and aggregate less, thus resulting in less dense fibrin network.

rate of longitudinal cross-linking within the fiber (γ-γ cross-links) is nearly the same as that of protofibril assembly, the first layer of protofibrils gets cross-linked as soon as they are assembled. In this nucleation layer, since the cross-linked protofibrils are stiffer, their more defined spatial orientation may facilitate the lateral aggregation and further growth. As the protofibrils are not bound to the FXIIIa-coated surface, the nucleation layer could be dynamic, i.e., it may be displaced from near the surface by the inward diffusive flux of a new set of uncross-linked protofibrils. The mobility of uncross-linked protofibrils to the surface results in a nucleation-elongation phenomenon akin to supramolecular, cooperative assembly of tubular polymers, wherein the first layer of monomers serves as a nucleation layer for additional monomers to attach and grow in three dimensions (42). Lastly, the protofibrils in the nucleation layer get further stabilized slowly by the transverse α-α cross-links.

Consistent with the fibrin deposition model based on reaction rates discussed above, the ultrastructure of the individual fibrin fibers near the microsphere surfaces provides insights into the mechanics of uncross-linked and partially cross-linked fibers. It has been shown that cross-linking by FXIIIa increases the compaction of protofibrils and, by preventing the protofibrils from sliding past each other, cross-linking increases the tensile stiffness, contractile stress, and shear stiffness by two- to threefold (28,38,43,44). We have recently shown that the lower stiffness of uncross-linked fibrin networks is attributable to their fourfold lower bending stiffness, which allows them to buckle and bend more readily than cross-linked fibers (27). As shown in Fig. 5, the uncross-linked fibrin fibers bound to the microspheres coated with anti-fibrin-E antibody are compliant with low bending stiffness, and are more branched, shorter, and tortuous. In contrast to these completely uncross-linked fibers, cross-linking even only a portion of the fibrin fibers by surface-immobilized FXIIIa decreases the curvature of the entire fiber segment by more than two orders of magnitude. The remarkable straightness of partially cross-linked fibers suggests that these fibers could have significantly higher bending stiffness than fully uncross-linked fibers (27,45). In fact, these fibrin fibers may consist of stiffer (cross-linked) segments close to the surface that transition into softer (uncross-linked) segments farther from the surface. The deposition of long straight fibers connecting two distant platelets also raises the intriguing possibility of long-range physical interaction between cells through the fibrin network (46). Our finding suggests that fibrin cross-linking may be crucial for cell-cell communication and platelet mechanotransduction.

In summary, we have shown that fibrin cross-linking by surface-bound FXIIIa leads to the formation of straighter, longer, and a thicker deposition of fibrin fibers compared with the binding of uncross-linked fibers to a surface. The kinetics of fiber deposition on FXIIIa-coated surfaces is suggestive of a localized interaction driven by cross-linking-induced compaction. This results in partially cross-linked fibers, which, despite not being bound to the surface, span several microns. Although the local stiffness of such hybrid fibers has not been measured experimentally, fiber networks with spatially varying stiffness have mechanobiological significance. In blood clots, FXIIIa expressed on the surface of activated platelets cross-links fibrin(ogen) bound to $\alpha_{IIb}\beta_3$ receptor, and is likely to strengthen the fibrin-$\alpha_{IIb}\beta_3$-myosin axis (47). This strengthening may arise from the locally increased stiffness of straighter and denser fibers in the immediate vicinity of platelets. Such fibrin bundles can be efficient in anchoring and transmitting the contractile forces exerted by the platelets, which are critical in the remodeling of fibrin during early-stage clot formation (26), late-stage clot contraction (24), outside-in mechanical signaling (48), and potentially mechanical communication between platelet aggregates (49). By isolating surface-bound FXIIIa from its counterpart in plasma, we have shown an important, but often overlooked, biophysical mechanism by which platelet-fibrin interaction may play a significant role in the mechanics of blood clots.

ACKNOWLEDGMENTS

We thank Dr. Danielle Jorgens and staff at UC Berkeley electron microscopy facility for technical assistance. The confocal microscopy at SJSU was made possible by an NSF MRI award (DBI-1229817), and SEM microscopy at UC Berkeley was made possible by NIH S10 award (S10OD030258-01).

AUTHOR CONTRIBUTIONS

M.A., M.P., and A.K.R. designed the experiments. M.A., M.P., and A.P.W. performed the experiments. M.A., M.P., S.-J.J.L., K.D., and A.K.R. analyzed the data and interpreted the results. M.A., M.P., and A.K.R. prepared the figures. A.K.R. conceived the project, acquired funding, and wrote the first version of the manuscript. M.A., M.P., S.-J.J.L., K.D., and A.K.R. prepared the final version of the manuscript.

DECLARATION OF INTERESTS

The authors declare no competing interests.

SUPPORTING MATERIAL

Supplemental information can be found online at https://doi.org/10.1016/j.bpr.2025.100207.

REFERENCES

1. Weisel, J. W., and R. I. Litvinov. 2017. Fibrin Formation, Structure and Properties. *In* Fibrous Proteins: Structures and Mechanisms. D. A. D. Parry and J. M. Squire, eds Springer International Publishing, pp. 405–455.
2. Brown, A. C., and T. H. Barker. 2014. Fibrin-based biomaterials: Modulation of macroscopic properties through rational design at the molecular level. *Acta Biomater.* 10:1502–1514.
3. Hickerson, W. L., I. Nur, and R. Meidler. 2011. A comparison of the mechanical, kinetic, and biochemical properties of fibrin clots formed with two different fibrin sealants. *Blood Coagul. Fibrinolysis.* 22:19–23.
4. Muszbek, L., Z. Bereczky, …, É. Katona. 2011. Factor XIII: A Coagulation Factor With Multiple Plasmatic and Cellular Functions. *Physiol. Rev.* 91:931–972.
5. Mitchell, J. L., and N. J. Mutch. 2019. Let's cross-link: diverse functions of the promiscuous cellular transglutaminase factor XIII-A. *J. Thromb. Haemostasis.* 17:19–30.
6. Braaten, J. V., R. A. Goss, and C. W. Francis. 1997. Ultrasound reversibly disaggregates fibrin fibers. *Thromb. Haemost.* 78:1063–1068.
7. Chernysh, I. N., C. Nagaswami, …, J. W. Weisel. 2012. Fibrin Clots Are Equilibrium Polymers That Can Be Remodeled Without Proteolytic Digestion. *Sci. Rep.* 2:879.
8. Carlisle, C. R., E. A. Sparks, …, M. Guthold. 2010. Strength and failure of fibrin fiber branchpoints. *J. Thromb. Haemostasis.* 8:1135–1138.
9. Liu, W., C. R. Carlisle, …, M. Guthold. 2010. The mechanical properties of single fibrin fibers. *J. Thromb. Haemostasis.* 8:1030–1036.
10. Mutch, N. J., J. S. Koikkalainen, …, N. A. Booth. 2010. Model thrombi formed under flow reveal the role of factor XIII-mediated cross-linking in resistance to fibrinolysis. *J. Thromb. Haemostasis.* 8:2017–2024.
11. Markert, C. D., X. Guo, …, M. Guthold. 2013. Characterizing the micro-scale elastic modulus of hydrogels for use in regenerative medicine. *J. Mech. Behav. Biomed. Mater.* 27:115–127.
12. Marta-Enguita, J., M. Navarro-Oviedo, …, J. Orbe. 2024. Role of factor XIII in ischemic stroke: a key molecule promoting thrombus stabilization and resistance to lysis. *J. Thromb. Haemostasis.* 22:1080–1093.
13. Tsurupa, G., S. Yakovlev, …, L. Medved. 2010. Noncovalent Interaction of α_2-Antiplasmin with Fibrin(ogen): Localization of α_2-Antiplasmin-Binding Sites. *Biochemistry.* 49:7643–7651.
14. Muszbek, L., R. A. Ariëns, and A. Ichinose. 2007. Factor XIII: recommended terms and abbreviations. *J. Thromb. Haemostasis.* 5:181–183.
15. Komáromi, I., Z. Bagoly, and L. Muszbek. 2011. Factor XIII: novel structural and functional aspects. *J. Thromb. Haemostasis.* 9:9–20.
16. Byrnes, J. R., C. Wilson, …, A. S. Wolberg. 2016. The interaction between fibrinogen and zymogen FXIII-A2B2 is mediated by fibrinogen residues γ390-396 and the FXIII-B subunits. *Blood.* 128:1969–1978.
17. Somodi, L., I. Beke Debreceni, …, L. Muszbek. 2022. Activation mechanism dependent surface exposure of cellular factor XIII on activated platelets and platelet microparticles. *J. Thromb. Haemostasis.* 20:1223–1235.
18. Muszbek, L., J. Polgár, and Z. Boda. 1993. Platelet Factor XIII Becomes Active without the Release of Activation Peptide during Platelet Activation. *Thromb. Haemost.* 69:282–285.
19. Mitchell, J. L., A. S. Lionikiene, …, N. J. Mutch. 2014. Functional factor XIII-A is exposed on the stimulated platelet surface. *Blood.* 124:3982–3990.
20. Mattheij, N. J. A., F. Swieringa, …, J. M. E. M. Cosemans. 2016. Coated platelets function in platelet-dependent fibrin formation

via integrin $\alpha_{IIb}\beta_3$ and transglutaminase factor XIII. *Haematologica.* 101:427–436.

21. Mitchell, J. L., G. Little, …, C. I. Jones. 2023. Platelet factor XIII-A regulates platelet function and promotes clot retraction and stability. *Res. Pract. Thromb. Haemost.* 7:100200.
22. Mitchell, J. L., and N. J. Mutch. 2016. Novel aspects of platelet factor XIII function. *Thromb. Res.* 141:S17–S21.
23. Michael, C., F. Pancaldi, …, M. Alber. 2023. Combined computational modeling and experimental study of the biomechanical mechanisms of platelet-driven contraction of fibrin clots. *Commun. Biol.* 6:869.
24. Sun, Y., D. R. Myers, …, A. Alexeev. 2021. Platelet heterogeneity enhances blood clot volumetric contraction: An example of asynchrono-mechanical amplification. *Biomaterials.* 274:120828.
25. Pathare, S. J., W. Eng, …, A. K. Ramasubramanian. 2021. Fibrin prestress due to platelet aggregation and contraction increases clot stiffness. *Biophys. Rep.* 1:100022.
26. Kim, O. V., R. I. Litvinov, …, J. W. Weisel. 2017. Quantitative structural mechanobiology of platelet-driven blood clot contraction. *Nat. Commun.* 8:1274.
27. Zakharov, A., M. Awan, …, K. Dasbiswas. 2024. Clots reveal anomalous elastic behavior of fiber networks. *Sci. Adv.* 10:eadh1265.
28. Nair, P. M., M. A. Meledeo, …, A. P. Cap. 2021. Cold-stored platelets have better preserved contractile function in comparison with room temperature-stored platelets over 21 days. *Transfusion (Paris).* 61:S68–S79.
29. HSIEH, L., and D. NUGENT. 2008. Factor XIII deficiency. *Haemophilia.* 14:1190–1200.
30. Jobe, S. M., L. Leo, …, J. Di Paola. 2005. Role of FcRγ and factor XIIIA in coated platelet formation. *Blood.* 106:4146–4151.
31. Evani, S. J., S. F. Dallo, …, A. K. Ramasubramanian. 2013. Shear Stress Enhances Chemokine Secretion from Chlamydia pneumoniae-infected Monocytes. *Cell. Mol. Bioeng.* 6:326–334.
32. Alshehri, F. S. M., C. S. Whyte, …, N. J. Mutch. 2021. Monocytes Expose Factor XIII-A and Stabilize Thrombi against Fibrinolytic Degradation. *Int. J. Mol. Sci.* 22:6591.
33. Mary, H., and G. J. Brouhard. 2019. Kappa (κ): Analysis of Curvature in Biological Image Data using B-splines. Preprint at bioRxiv. https://doi.org/10.1101/852772.
34. Törőcsik, D., H. Bárdos, …, R. Ádány. 2005. Identification of factor XIII-A as a marker of alternative macrophage activation. *Cell. Mol. Life Sci.* 62:2132–2139.
35. Muszbek, L., R. Adány, …, M. Kávai. 1985. Factor XIII of blood coagulation in human monocytes. *Thromb. Res.* 37:401–410.
36. Lishko, V. K., N. P. Podolnikova, …, T. P. Ugarova. 2004. Multiple binding sites in fibrinogen for integrin alphaMbeta2 (Mac-1). *J. Biol. Chem.* 279:44897–44906.
37. Morris, A. M., M. A. Watzky, …, R. G. Finke. 2008. Fitting Neurological Protein Aggregation Kinetic Data via a 2-Step, Minimal/"Ockham's Razor" Model: The Finke–Watzky Mechanism of Nucleation Followed by Autocatalytic Surface Growth. *Biochemistry.* 47:2413–2427.
38. Kurniawan, N. A., J. Grimbergen, …, G. H. Koenderink. 2014. Factor XIII stiffens fibrin clots by causing fiber compaction. *J. Thromb. Haemostasis.* 12:1687–1696.
39. Lewis, S. D., P. P. Shields, and J. A. Shafer. 1985. Characterization of the kinetic pathway for liberation of fibrinopeptides during assembly of fibrin. *J. Biol. Chem.* 260:10192–10199.
40. Kelley, M. A., and K. Leiderman. 2022. Mathematical modeling to understand the role of bivalent thrombin-fibrin binding during polymerization. *PLoS Comput. Biol.* 18:e1010414.
41. Lewis, K. B., D. C. Teller, …, P. D. Bishop. 1997. Crosslinking kinetics of the human transglutaminase, factor XIII[A2], acting on fibrin gels and gamma-chain peptides. *Biochemistry.* 36:995–1002.
42. Zhao, D., and J. S. Moore. 2003. Nucleation–elongation: a mechanism for cooperative supramolecular polymerization. *Org. Biomol. Chem.* 1:3471–3491.
43. Standeven, K. F., A. M. Carter, …, R. A. S. Ariëns. 2007. Functional analysis of fibrin {gamma}-chain cross-linking by activated factor XIII: determination of a cross-linking pattern that maximizes clot stiffness. *Blood.* 110:902–907.
44. Liu, W., C. R. Carlisle, M. Guthold…, 2010. The mechanical properties of single fibrin fibers. *J. Thromb. Haemostasis.* 8:1030–1036.
45. Piechocka, I. K., R. G. Bacabac, …, G. H. Koenderink. 2010. Structural hierarchy governs fibrin gel mechanics. *Biophys. J.* 98:2281–2289.
46. Notbohm, J., A. Lesman, …, G. Ravichandran. 2015. Microbuckling of fibrin provides a mechanism for cell mechanosensing. *J. R. Soc. Interface.* 12:20150320.
47. Kasahara, K., M. Kaneda, …, N. Yamamoto. 2013. Clot retraction is mediated by factor XIII-dependent fibrin-αIIbβ3-myosin axis in platelet sphingomyelin-rich membrane rafts. *Blood.* 122:3340–3348.
48. Chen, Y., L. A. Ju, …, C. Zhu. 2019. An integrin αIIbβ3 intermediate affinity state mediates biomechanical platelet aggregation. *Nat. Mater.* 18:760–769.
49. Qiu, Y., A. C. Brown, …, W. A. Lam. 2014. Platelet mechanosensing of substrate stiffness during clot formation mediates adhesion, spreading, and activation. *Proc. Natl. Acad. Sci. USA.* 111:14430–14435.